



Role of the Fe-zeolite structure and iron state in the N₂O decomposition: Comparison of Fe-FER, Fe-BEA, and Fe-MFI catalysts

K. Jíša, J. Nováková, M. Schwarze, A. Vondrová, S. Sklenák, Z. Sobalik*

J. Heyrovský Institute of Physical Chemistry, Academy of Sciences of the Czech Republic, Dolejškova 3, 182 23 Prague 8, Czech Republic

ARTICLE INFO

Article history:

Received 25 July 2008

Revised 7 November 2008

Accepted 21 November 2008

Available online 7 January 2009

Keywords:

Fe in FER

BEA and MFI

N₂O decomposition

ABSTRACT

The decomposition of nitrous oxide was compared over Fe-FER, Fe-MFI, and Fe-BEA with well established iron distribution in cationic positions and low amounts of less well-established oxide species. It was evidenced that, despite a comparable content of Fe(II) in the cationic positions, the catalytic activity of Fe-FER greatly exceeds that of Fe-BEA and Fe-MFI. While about one half of the iron sites in Fe-FER (Fe/Al < 0.15) participate in the decomposition of nitrous oxide after activation at 450 °C, the number of active sites in Fe-BEA or Fe-MFI was much lower, and, accordingly, without acceleration of the reaction by the addition of NO, these samples exhibit much lower catalytic activity than Fe-FER. This could be likely correlated with the concentration of Fe(II) in positions with a specific spatial iron arrangement at optimal Fe···Fe distances. For that role we propose a local structure with two adjacent β sites, where the Fe···Fe distance would be 7 to 7.5 Å, i.e. comparable to the length of the N₂O molecule, and provide potential for cooperation of the two iron cations on the N₂O molecule splitting. Such arrangement is absent in both the Fe-BEA and Fe-MFI structures.

© 2008 Elsevier Inc. All rights reserved.

1. Introduction

Iron-containing zeolites are known as excellent catalysts for the decomposition of harmful nitrous oxide to nitrogen and oxygen. Since the original experiments of Panov's [1] laboratory, the greatest attention has been paid to iron in MFI structures. Summarization of numerous experimental and theoretical studies of Fe in MFI structures, various means of preparation and pretreatment, the reaction mechanism and practical utilization are beyond the scope of this paper (see, e.g., Refs. [2–6]). Far fewer studies are concerned with the decomposition of N₂O over iron in other zeolite structures compared to Fe-MFI: Cabrera [7] reports on the excellent activity and durability of Fe-FER in N₂O decomposition under conditions in nitric acid plants. The highest activity in direct N₂O decomposition of commercial BEA compared to FER and MFI (in H-forms), all with iron impurities, was found by Oygarden and Pérez-Ramírez [8]. An advantage of Fe-BEA over FeZSM-5, both prepared by wet ion exchange, was found by Pieterse et al. [9] and ascribed to the highly dealuminated parent BEA zeolite. Comparing Fe-MFI and Fe-BEA, Pérez-Ramírez et al. [10] claimed that the microporous matrix does not play a decisive role in the decomposition of N₂O, provided similar forms of iron are present in the final catalyst. Mauvezin et al. [11] studied Fe-BEAs with different Fe loading. Lázár

et al. [12] used MSB to study Fe-FER in which iron was introduced into framework positions during synthesis and its location was further altered during subsequent treatment. The properties of iron in various zeolite structures, mainly in FER, BEA and MFI, have been extensively studied in our group: IR spectra of skeletal vibrations revealed the presence of three cationic sites (α , β , and γ) with preferential occupation of β sites at low iron loading [13–16], and further confirmed by MSB studies [17], and by periodic DFT calculations [18–20]; the effect of NO assisted N₂O reaction and role of NO were analyzed in Refs. [21–26]. Moreover, two review papers evaluated the subject have appeared recently [4,25].

The present study contributes to assessment of the potential of various iron-containing zeolites for N₂O decomposition and of the relationship between their catalytic performance and their specific structures. Several characterizing methods are used to identify the individual iron forms in Fe-zeolites treated under various conditions, mainly temperature-programmed reduction (TPR) and Mössbauer spectroscopy (MSB). Previous results of Fe-FER characterization by of MSB [17] and FTIR, UV/vis and ESR [13,21] for Fe-zeolites are also employed.

Zeolites with relatively low Si/Al values (8.5–15) and low contents of iron cations were used to check the effect of the structural features of the individual zeolites on the catalytic activity in the N₂O decomposition. The concentration differences between the individual Fe-samples are, to some extent, eliminated by their very similar Fe/Al ratios (0.11–0.13). The use of MSB enables to directly checking for the presence of oxidic Fe species. Comparison of the

* Corresponding author. Fax: +420 286582307.

E-mail address: zdenek.sobalik@jh-inst.cas.cz (Z. Sobalik).

total consumption of hydrogen during the TPR and that related to Fe cations provides additional information on the individual Fe species. For comparison, Fe-FER and Fe-BEA with higher iron loading were also examined.

The distances between the individual cationic sites as well as their geometry were analyzed using the Materials Studio, release 4.3, from Accelrys.

Attention has also been paid to the effects of zeolite pretreatment at high temperatures and to the presence of NO during the decomposition of nitrous oxide. While the standard arrangement of the catalytic test consisted in a flow-through micro-reactor, a batch reactor with MS (mass spectrometry) was also employed to study the isotopic exchange of $^{15}\text{N}_2^{18}\text{O}$ with zeolitic oxygen and to identify the desorbed products of surface species created by the N_2O decomposition and their relevance for the catalytic process.

2. Experimental

2.1. Zeolites

FER (Tosoh, Japan; Si/Al 8.6), BEA (Zeolyst; Si/Al 15.5), and MFI (VURUP, SR; Si/Al 13.4) were used as parent zeolites for the catalyst preparation. The method for introduction of iron has been reported previously in detail [27]. The procedure was based on impregnation of the parent ammonia zeolite form by an FeCl_3 solution in acetyl-acetone, followed by calcination in an air flow at 420°C for 10 h. Samples with a low Fe/Al ratio of ~ 0.1 have mostly been prepared. These Fe/Al ratios are only slightly higher than those typical for maximum N_2O decomposition related to the iron content [25]. In some cases, also samples with higher Fe loading (up to Fe/Al of 0.47) have been included for comparison. For the MSB analysis, iron samples with high enrichment of the ^{57}Fe isotope ($^{57}\text{Fe} > 98$ wt% in Fe_2O_3 , supplied by ISOFLEX, USA) were prepared by the same procedure. The chemical analysis was carried out at Research Institute of Inorganic Chemistry, CR, using a Philips PW 1404 XRF spectrometer.

2.2. TPD procedure

The samples (100 mg) were placed in a vacuum cell and dehydrated at 150°C in vacuum for 1 h and then heated in a vacuum with a temperature ramp of 5°C min^{-1} either to 450°C (LTP, low-temperature pretreatment) or to 700°C (HTP, high temperature pretreatment). The released gases were introduced directly into a Balzers QMG 420 quadrupole mass spectrometer. Molecular ions of hydrogen, water, oxygen, carbon mono- and dioxide were recorded. The same procedure was used to identify the gases released from surface species formed by the interaction of nitrous oxide at different temperatures over LTP or HTP samples. Molecular ions corresponding to oxygen, nitrous oxide, nitric oxide and nitrogen dioxide (fragmentation corrected) were recorded. Pure compounds were employed for the calibration.

2.3. Mössbauer spectroscopy

^{57}Fe was ion-exchanged into NH_4 zeolites by the above-described methods. A self-supported pressed target (ca. 50 mg cm^{-2}) was placed in a laboratory-made vacuum cell providing for transport of the sample between the heated to measuring positions. The absorption spectra were recorded at room temperature under maximum velocity of the source of 12 mm s^{-1} , using ^{57}Co in a Rh matrix. The velocity scale was calibrated using $\alpha\text{-Fe}$. The experimental details were described in the previous paper [17]. LTP and HTP samples were pretreated in situ in vacuum or further oxidized by oxygen at 450°C and/or by nitrous oxide at 250°C . The spectra were analyzed assuming Lorentzian linear profiles of individual components, and using the NORMOS program.

2.4. TPR

TPR experiments were carried out using an Altamira AMI 200 instrument. The catalyst (typically 100 mg) was placed in a quartz micro-reactor located in a furnace and pretreated under various conditions described below. Reduction by hydrogen was carried out in a H_2/Ar stream (9.44 vol% of H_2), with a total flow rate of 30 ml min^{-1} and a linear heating rate of $20^\circ\text{C min}^{-1}$ in the temperature range $35\text{--}800^\circ\text{C}$.

Individual pretreatment *in situ* prior to TPR was as follows:

- (i) Oxidation in the air: Air flow with a flow rate of 30 ml min^{-1} , temperature ramp of $10^\circ\text{C min}^{-1}$ up to 450°C (LTP samples), then stabilized for 1 h, at this temperature, and cooled in the air to room temperature (RT).
- (ii) Treatment in Ar: Argon flow of 30 ml min^{-1} , temperature ramp of $10^\circ\text{C min}^{-1}$ up to 700°C (HTP samples), then stabilized at this temperature for 2 h, cooled in Ar to RT or 200°C .
- (iii) Oxidation in N_2O : The pretreated samples were exposed to a stream of N_2O (flow 30 ml min^{-1}) at 200°C for 1 h, and then cooled to RT.

The TPR curves were integrated using the Origin software.

2.5. Catalytic tests— N_2O decomposition, flow experiments

The reaction was performed in a temperature range of $200\text{--}450^\circ\text{C}$ using a standard U-shaped flow reactor. Before the catalytic test, the sample was pretreated *in situ* in a helium stream at 450°C for 2 h, followed by treatment in an oxygen stream for 1 h at the same temperature (LTP samples), or at 700°C (HTP samples). Nitrous oxide (1000 ppm) and carrier gas (helium), in specified experiments with addition of 500 ppm of NO, were mixed using a setup of several mass-flow controllers (ELMET, CZ and KARA, CZ). The overall flow rate was kept between $300\text{ cm}^3\text{ min}^{-1}$, i.e. the GHSV was approx. $90,000\text{ h}^{-1}$. Analysis of the gas composition at the reactor outlet was performed using an Advance Optima IR analyzer (ABB Co., Germany) for N_2O , and a chemiluminescence analyzer (VAMET, CZ) for NO and NO_2 . N_2 and O_2 were analyzed using a Hewlett-Packard 5890 II GC chromatograph.

2.6. Catalytic tests— N_2O decomposition, batch experiments

The reaction was carried out in a reaction vessel (175 cm^3) at 280°C and, in some cases, also at 200 or 250°C . The LTP samples were pretreated *in situ* in vacuum at 450°C (LTP samples) or 700°C (HTP samples) for 2 h and then cooled to 280°C . Nitrous oxide (500 Pa) was allowed to react with the pretreated sample at 280°C for 70 min. In some cases, a mixture of 500 Pa of N_2O and 50 Pa of NO was used. A negligible part of the reaction mixture was introduced into a QMG 420 quadrupole mass spectrometer using a needle valve. The mass spectrometer was calibrated using individual reaction components. After reaction for 70 min, the gas phase was briefly evacuated, the sample was cooled to 150°C or to room temperature (RT), and surface species left after the reaction were decomposed using the TPD procedure.

2.7. Structural analysis of the potential active sites

The distances between of the individual cationic sites as well their geometry were analyzed using the Materials Studio, release 4.3, from Accelrys. The structures of individual zeolites were taken from optimized structures obtained by periodic DFT calculations [18,19] or from data provided in the literature [28].

Table 1
Chemical composition of studied zeolites.

Sample	Si/Al	Fe ($\mu\text{mol g}^{-1}$)	Fe/Al
FER _{parent}	8.6	18	0.01
Fe-FER _{0.12}	8.7	175	0.12
Fe-FER _{0.26}	8.7	376	0.26
^a Fe-FER _{0.08}	8.4	111	0.08
Fe-FER _{0.47}	8.9	652	0.47
BEA _{parent}	15.5	63	0.07
Fe-BEA _{0.13}	15.3	109	0.13
^a Fe-BEA _{0.12}	15.5	106	0.12
Fe-BEA _{0.32}	15.3	268	0.32
MFI _{parent}	13.4	25	0.02
Fe-MFI _{0.11}	13.4	113	0.11
^a Fe-MFI _{0.14}	13.4	161	0.14

^a ⁵⁷Fe samples.

3. Results

3.1. Sample characterization

3.1.1. Characterization of prepared Fe-zeolites

The chemical composition of the samples is summarized in Table 1. The Si/Al ratios are in the region of low Si/Al values typical for the individual zeolite structures. The samples of Fe zeolites are further denoted by an index indicating the Fe/Al ratio, e.g. Fe-FER_{0.12}.

3.1.2. TPD—gases released during the LTP and HTP processes

The treatment up to 450 °C (LTP samples) mostly leads to dehydration of the sample, while the treatment at temperatures around 700 °C (HTP samples) results in deep dehydroxylation and formation of defects of a Lewis nature (e.g. [21–25,29]). Only water vapor is released during the HTP treatment of Fe-FER_{0.12}, while Fe-FER with higher Fe loading also evolves oxygen. On the other hand, Fe-BEA_{0.13} and Fe-MFI_{0.11} with compositions similar to Fe-FER_{0.12} release much more O₂, in amounts comparable to Fe-FER_{0.26}. We assume that the appearance of oxygen released from the analyzed samples could be correlated with the presence of iron in non-cationic positions, probably as iron oxides. We have not found release of hydrogen from our Fe-zeolites, contrary to the findings of Nash et al. [30], who report its formation from H-ZSM-5 in a similar experimental arrangement.

3.1.3. MSB results

Fig. 1 summarizes the MSB spectra of the samples evacuated at 450 (LTP) or 700 °C (HTP), as well as the LTP samples after oxidation by oxygen at 450 °C.

For interpretation of the MSB results over iron-zeolites, we generally accept the assignment proposed by Ovanesyan et al. [31–33]: iron holding the active oxygen is characterized by two doublets with IS (isomer shift) above 1.0, and parameters of QS (quadrupole splitting) are characterized roughly in two regions, above 1.5 (“O_h-like species”) or below 1.0 (“T_h-like species”). However, we do not accept the proposed true O_h or T_d coordinations for iron cations as this coordination would not be possible for divalent cations in the cation positions of MFI or the other two studied zeolites. IS below 0.5 in the spectra are assigned to Fe(III) species.

All three LTP and HTP Fe-zeolites treated in vacuum contain iron predominantly in the Fe(II) oxidation state bonded in cationic forms (see Table 2). As indicated by the spectral analysis, at least two individual Fe(II) forms prevail in the Fe-FER (IS = 0.94 mm s⁻¹, QS = 0.69 mm s⁻¹ and IS = 1.18 mm s⁻¹, QS = 2.04 mm s⁻¹), Fe-BEA (IS = 0.88 mm s⁻¹, QS = 0.61 mm s⁻¹; IS = 0.80 mm s⁻¹, QS = 1.85 mm s⁻¹) and Fe-MFI (IS = 1.06 mm s⁻¹, QS = 1.59 mm s⁻¹; IS = 0.89 mm s⁻¹, QS = 0.74 mm s⁻¹). The form with lower QS prevails in Fe-FER (65 vs. 31%), while the

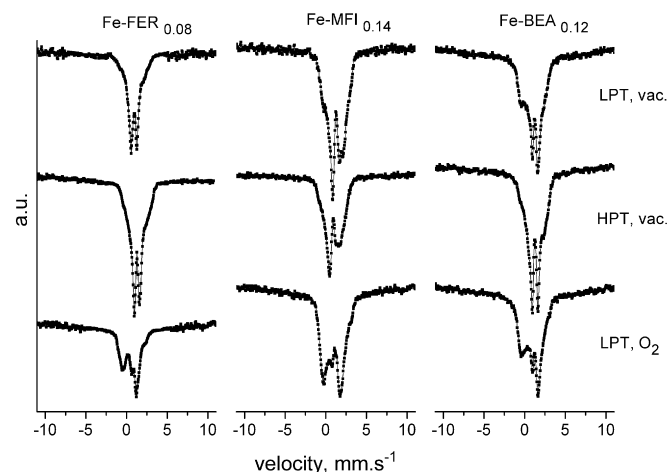


Fig. 1. MSB spectra of Fe/zeolites pretreated in vacuum at 450 and 700 °C and in oxygen at 450 °C.

Table 2

Concentration of Fe(II) in Fe-zeolite samples after evacuation at 450 °C and after following oxidation by oxygen at the same temperature, as revealed by MSB measurements.

	Concentration of Fe(II) after evacuation at 450 °C		Concentration of Fe(II) after oxidation by O ₂ at 450 °C	
	c _{Fe(II)} /c _{Fe tot}	c _{Fe(II)} ($\mu\text{mol g}^{-1}$)	c _{Fe(II)} /c _{Fe tot}	c _{Fe(II)} ($\mu\text{mol g}^{-1}$)
Fe-FER _{0.08}	0.96	106.6	0.33	37
Fe-MFI _{0.14}	0.81	130	0.70	113
Fe-BEA _{0.12}	0.88	126	0.73	104

forms with higher QS are more abundant in both MFI (45 vs. 22%) and BEA (64 vs. 20%).

A much lower concentration (~3–5%) of additional cationic form has been tentatively indicated in the spectra of Fe-MFI and Fe-BEA.

MSB spectra reveal, in agreement with the IR data and DFT calculations [13–16,18–20] that the cationic form predominates in all three zeolites. The approach to direct assignment of the individual iron species—i.e. occupation of the individual cationic sites and their assignment in the MSB spectra of the individual iron zeolites will be published elsewhere. For the purpose of the present analysis, we do not distinguish between the individual Fe cationic forms, and only the correlation between the total amount of cationic Fe(II) and the catalytic data will be discussed. Nevertheless, we consider it to be significant that the amount of the Fe(II) cationic forms in the LTP and HTP samples treated in vacuum (Table 2) corresponds to the sequence:

Fe-FER > Fe-BEA ≥ Fe-MFI.

According to the MSB spectra, a significant difference occurs between the individual iron-zeolites after oxidation by oxygen at 450 °C. Namely, the part of the Fe(II) cationic species resisting oxidation (Table 2) depends on the type of zeolite in a sequence opposite to that after the pretreatment in vacuum:

Fe-MFI ~ Fe-BEA ≫ Fe-FER.

The increase in the temperature of evacuation to 700 °C (HTP) leads to only a limited change in the ratio of Fe(II) and Fe(III) oxidation states [17].

During the treatment in N₂O at 250 °C, practically all Fe(II) ions are oxidized to Fe(III) in the above Fe-zeolites.

3.1.4. TPR

The TPR results for iron-zeolites are presented in Figs. 2 and 3. The reduction of all the iron zeolites proceeds basically in two

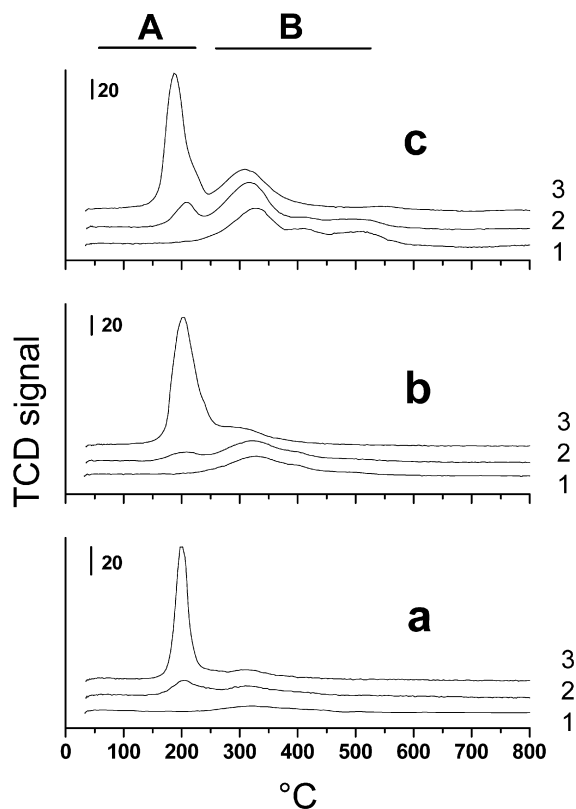


Fig. 2. TPR spectra of Fe-FERs. Spectra 1, 2 and 3 were taken after pretreatment of the LTP sample in oxygen at 450 °C, of the LTP sample after oxidation by N₂O at 200 °C, and of the HTP sample after oxidation by N₂O at 200 °C, respectively.

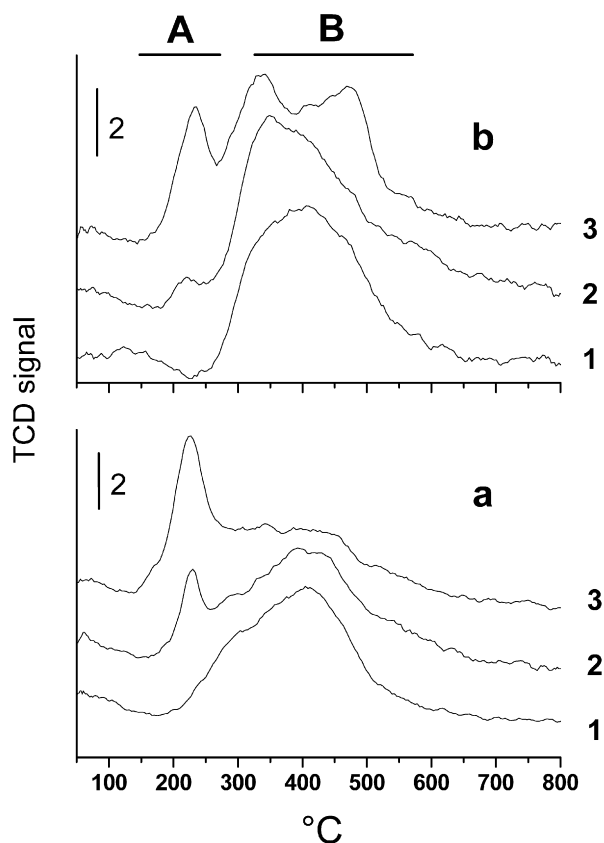


Fig. 3. TPR spectra for Fe-MFI and Fe-BEA: (a) Fe-MFI_{0.11}, (b) FeBEA_{0.13}. Curves 1–3: after the same treatment as in Fig. 2.

Table 3

Consumption of hydrogen in the **A** and **B** regions for the LTP samples oxidized by N₂O at 200 °C, compared to the amount of iron.

Fe-zeolites, TPR	Conc. Fe (μmol g ⁻¹)	H ₂ consumption (μmol g ⁻¹)		H ₂ /Fe ratio ^a
		A region	B region	
Fe-FER _{0.12}	175	33.4	38.7	0.41
Fe-FER _{0.26}	376	32.2	160.3	0.51
Fe-FER _{0.47}	652	22.2	380.3	0.62
Fe-BEA _{0.13}	109	2.4	61.2	0.58
Fe-MFI _{0.11}	113	7.4	57.2	0.57

^a Calculated as the sum of the H₂ consumption in the **A** and **B** regions by the total iron content.

Table 4

The consumption of hydrogen in the **A** and **B** region over the HTP samples oxidized by N₂O at 200 °C compared with the amount of iron.

Fe-zeolites, TPR	Amount of Fe (μmol g ⁻¹)	TPR, H ₂ consumption (μmol g ⁻¹)		H ₂ /Fe ratio ^a
		A region	B region	
Fe-FER _{0.12}	175	154	32	1.06
Fe-FER _{0.26}	376	243	144	1.03
Fe-FER _{0.47}	652	315	263	0.89
Fe-BEA _{0.13}	109	12.4	68.9	0.75
Fe-MFI _{0.11}	113	19.3	38.5	0.51

^a Calculated as sum of H₂ consumption in the **A** and **B** regions by the total iron content.

temperature regions, i.e. in the low temperature region 50–250 °C (denoted further in the text as region **A**) and at temperatures of 250–500 °C (denoted as region **B**). Reduction in the **B** region can be mostly due to Fe-oxidic species. The pretreatment in nitrous oxide results in a TPR peak in the **A** region, which can be related to the reduction of oxygen captured on Fe cations during the N₂O treatment. We denote this oxygen as O_{act} to distinguish it from other oxidic forms (see, e.g. [34]).

The TPR of Fe-FER with different iron loadings after pretreatment of the LTP samples in oxygen, and of the LTP and HTP samples in nitrous oxide, are depicted in Fig. 2. After oxidation in the air, all the Fe-FER samples exhibit hydrogen consumption only in the **B** region, and the hydrogen consumption increases with iron loading. The reduction peak in the **A** region increases substantially after the HTP treatment.

The TPR spectra of Fe-MFI and Fe-BEA are depicted in Fig. 3: the consumption of hydrogen over the samples pretreated in oxygen at 450 °C (region **B**) is much higher than that for Fe-FER samples. Reduction in the **A** region after oxidation by N₂O is considerably lower for both the Fe-BEA and Fe-MFI samples, but also leads to hydrogen consumption in the **B** region. The HTP pretreatment increases the reduction in the **A** region over samples oxidized by N₂O to a much lower extent than over Fe-FER.

The calculated hydrogen consumption in the TPR experiments after the oxidation by oxygen and by N₂O in the LTP samples is listed in Table 3.

It can be seen that the consumption of hydrogen in the **A** region is the highest for the Fe-FER sample with low Fe/Al value, and relatively decreases with the iron content in Fe-FER. The consumption of hydrogen is considerably lower in the **A** region for Fe-MFI and Fe-BEA, but higher in the **B** region.

Nevertheless, the ratio of hydrogen consumed in both temperature regions per iron present in all samples is similar and stabilized between 0.4 and 0.6.

The consumption of hydrogen over the HTP samples is listed in Table 4.

The total amount of captured O_{act} substantially increases after the HTP treatment; for the two Fe-FERs with low Fe/Al ration it approaches a value of 1, which indicates complete oxidation of all the iron present. Moreover, for Fe/FER_{0.12}, the proportion of the O_{act} is close to 90% of all the iron cations present. This is not the case for the Fe-FER samples with increasing iron content. HTP treatment

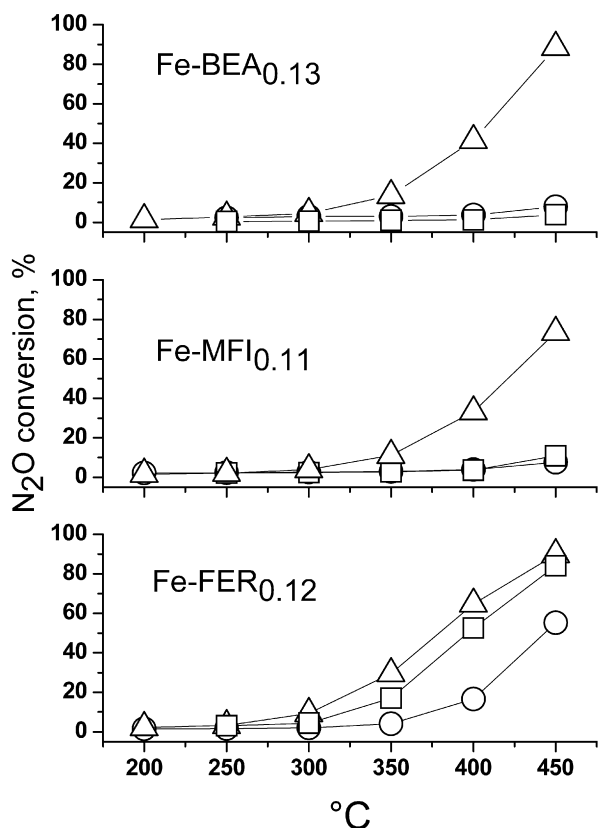


Fig. 4. Temperature dependence of the N₂O conversion, flow experiments: (○) N₂O alone over LTP samples, (□) N₂O alone over HTP samples, (△) N₂O + NO over LTP samples.

also increases the H₂ consumption in the **A** region for Fe-BEA and Fe-MFI, but the absolute values are still much lower than that for Fe-FER.

3.1.5. TPD after N₂O decomposition at 200 °C for 70 min

The amounts of desorbed oxygen after this reaction exhibit the same trend as the consumption of hydrogen in the **A** region (the data are compared in the survey, see Fig. 7).

3.2. Catalytic tests—N₂O decomposition

3.2.1. N₂O decomposition—flow experiments over Fe-zeolites with low Fe/Al ratios

The temperature dependence of conversion over all three iron zeolites is summarized in Fig. 4. Obviously, without addition of NO, the catalytic activity for the N₂O decomposition below 400 °C is manifested only over the Fe-FER sample. Moreover, the Fe-FER sample is unique in its response to the HTP treatment. It can be seen that the HTP treatment has a strong enhancing effect on the N₂O conversion over Fe-FER_{0.12}, nearly the same as the effect of addition of NO. On the other hand, for low iron-containing MFI and BEA samples, the HTP treatment has only a limited effect, and their activity could be increased only by the addition of nitric oxide (see further).

3.2.2. N₂O decomposition—batch experiments

The extent of decomposition of nitrous oxide at 280 °C after 70 min for individual iron-zeolites indicates the same trend in catalytic activities as in the flow experiments, i.e. the highest conversion over Fe-FER_{0.12}, low effect of the HTP treatment on Fe-BEA_{0.11} and Fe-MFI_{0.17}, and the positive effect of NO addition for all the Fe-samples used. Fe-FER samples with higher Fe loading exhibit

slightly greater activity in the decomposition of nitrous oxide than Fe-FERs with Fe/Al ≤ 0.12.

Reversibility of the effect induced by the HTP pretreatment was checked on the Fe-FER samples rehydrated after the previous HTP treatment by exposure to moisture at RT. The increased activity of Fe-FER_{0.12} observed after HTP treatment has been shown to be decreased to the original values after rehydration. However, such reversibility is less pronounced for Fe-FER with higher iron loading (Fe/Al > 0.15), and the higher activity of the HTP treated sample is partially preserved after the rehydration.

3.2.3. Effect of the addition of NO

Addition of NO substantially increases the conversion of nitrous oxide over all three iron zeolites (see Fig. 4). The effect of the NO amount differs between Fe-FER and Fe-MFI, Fe-BEA (to be discussed elsewhere).

Nevertheless, there is a basic difference in the response of the three different iron-zeolite systems to an increasing amount of added NO: while the addition of a relatively small amount of NO (50 ppm of NO vs. 1000 ppm of N₂O) substantially increases the conversion of N₂O over Fe-FER and a further increase of the amount of NO added has only a limited effect, conversion of N₂O over Fe-MFI and Fe-BEA increases steadily with an increase in the NO concentration in a broad concentration range. This obviously indicates a basically different process of the functioning of NO in the N₂O decomposition over these three zeolites.

NO_x surface species play nevertheless an important role in all three Fe-zeolites. The active role of NO_x surface species, either formed during the decomposition of N₂O alone or produced by addition of NO during the NO-assisted N₂O decomposition over Fe-FER was reported in Refs. [21–25,29]. The effect of NO_x surface species on the N₂O decomposition was also checked over Fe-BEA and Fe-MFI; their presence substantially increased the decomposition of nitrous oxide.

3.2.4. TPD products after the batch N₂O decomposition

The obvious crucial role of the surface NO_x species in the N₂O decomposition makes it important to identify the differences in their amounts over the individual iron-zeolites, after both the LTP and the HTP pretreatment. The products of the decomposition of the surface species that accumulated during the N₂O reaction over iron-zeolites are depicted in Fig. 5, in the upper part for the LTP Fe-zeolites and in the bottom part for the HTP samples.

The total amount of species desorbed from the LTP samples after the N₂O decomposition decreases in the order Fe-FER > Fe-BEA ≫ Fe-MFI. The amount of desorbed NO is similar for Fe-FER and Fe-BEA, and much lower for Fe-MFI.

Products desorbing from samples after the HTP treatment are in different proportions, namely the fraction of desorbed NO increases over all three Fe-zeolites and, more significantly, the surface NO_x species are much more strongly bonded, as indicated by a substantial shift in the desorption temperature of NO to well above 350 °C. This could be directly correlated with the established role of surface NO_x species in the N₂O decomposition [21–25] and thus with the higher activity of the HTP Fe-zeolites; Fe-FER again exhibits the highest activity and the highest amount of desorbed NO. Moreover, it has been previously shown, using ¹⁸O labeled nitrous oxide, that the participation of the framework oxygen in O₂ formation is suppressed over HTP treated zeolites; ¹⁸O₂ predominates over ¹⁸O¹⁶O and ¹⁶O₂ in the products, i.e. both oxygen atoms come directly from N₂¹⁸O [22,25,29].

The sequence of dioxygen isotopomers released during the decomposition of N₂¹⁸O at 280 °C over LTP Fe-zeolites is shown in Fig. 6, together with the change in ¹⁸O with the time of the reaction. Isotopomer ¹⁶O¹⁸O predominates in all the samples, which means that, on the one hand, zeolitic oxygens participate in the

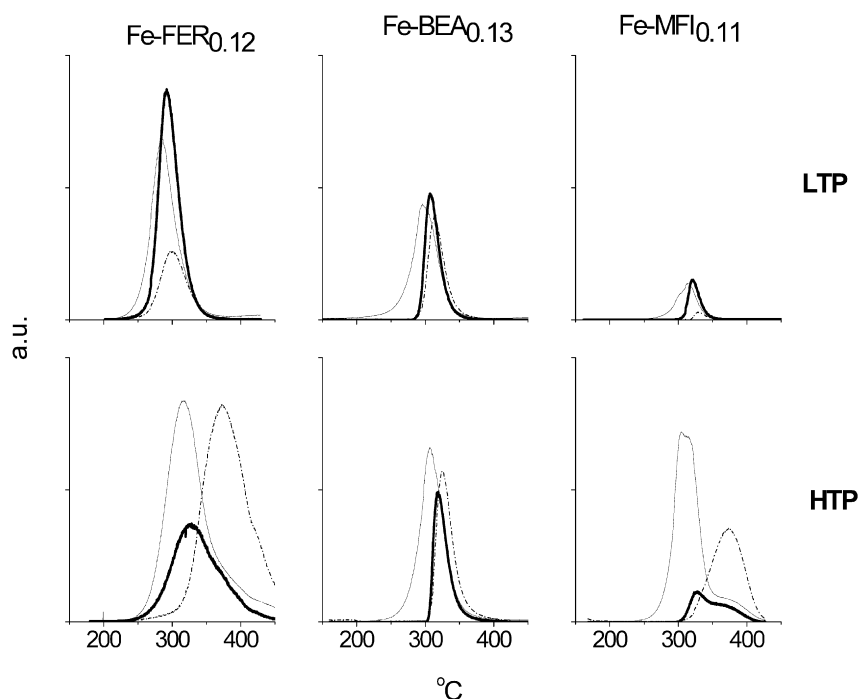


Fig. 5. TPD products after N_2O decomposition at 280°C , batch experiments: upper part for the LTP samples, bottom part for the HTP samples, thin curves for O_2 , bold curves for NO_2 , dash-dotted curves for NO .

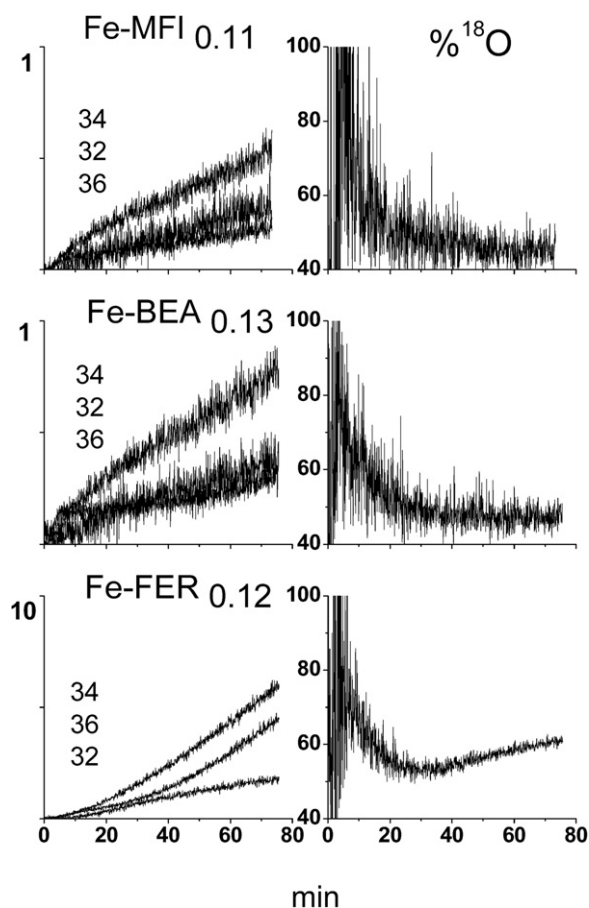


Fig. 6. Oxygen isotopomers released during $^{15}\text{N}_2$ ^{18}O decomposition at 280°C , and ^{18}O concentration, batch experiments. Left-hand side: oxygen isotopomers, denoted in descending order by m/z ratios, where 32 stands for $^{16}\text{O}_2$, 34 for $^{16}\text{O}^{18}\text{O}$ and 36 for $^{18}\text{O}_2$. Right hand-side: ^{18}O concentration in dioxygen.

reaction, and, on the other hand, the isotopic exchange most probably proceeds in one interaction step, i.e. $\text{N}_2^{18}\text{O} + ^{16}\text{O}$ zeol \rightarrow $\text{N}_2 + ^{16}\text{O}^{18}\text{O}$. The amount of skeletal oxygens participating in the O_2 formation, calculated from the total amount of ^{18}O in the products after 70 min of the reaction at 280°C equals to $130 \mu\text{mol g}^{-1}$ for the Fe-FER, and to $110 \mu\text{mol g}^{-1}$ for Fe-MFI and Fe-BEA. The number of participating zeolite oxygens is thus not very different for all Fe-zeolites, despite the considerably lower extent of nitrous oxide decomposition over the latter two samples. For comparison, Fe-FER $_{0.26}$ and Fe $_{0.47}$ indicate the participation of 176 and $191 \mu\text{mol g}^{-1}$ zeolite oxygens, respectively. This roughly agrees with the increased N_2O conversion over these Fe-FER samples.

4. Discussion

It is commonly accepted that in zeolites exist several forms of iron, depending on the preparation process, iron loading and treatment (e.g. [1–20]). A relationship has been already proposed between the catalytic activity of iron zeolites in the decomposition of nitrous oxide and the total amount of iron present in the cationic positions of the zeolite [4,13–20].

Nevertheless, for the N_2O decomposition in the absence of NO , there is no such straightforward correlation which would include all three Fe-zeolites. Actually, despite higher efficiency in occupation of the cationic positions in FER, the absolute amount iron in the cationic positions in all three zeolites is quite comparable and, taking into consideration only the Fe(II) resisting oxidation by an oxygen molecule, it could even be reversed, indicating that Fe-FER has a relatively lower amount of such iron cationic positions.

It is not surprising that there is no good correlation between the total amount of oxygen retained (i.e. a sum of consumed hydrogen in **A** and **B** regions) by the sample as a result of interaction with N_2O and the catalytic activity. Actually, on Fe-BEA $_{0.13}$ and Fe-MFI $_{0.11}$, most of the reduction occurs at high temperatures. However, by taking into account the amount of easily removable O_{act} (**A** region), a rather good correlation with the catalytic data for simple N_2O decomposition is obtained for all zeolites. This is

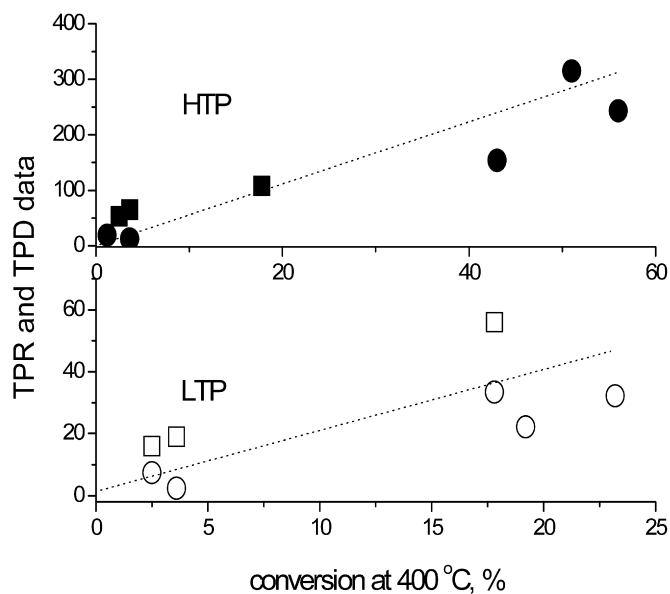


Fig. 7. Conversion of N_2O at $400\text{ }^\circ\text{C}$ vs. consumption of hydrogen in the A region and vs. desorbed oxygen after the N_2O interaction: (○) for TPR data, (□) for desorbed oxygen; (bottom) LTP Fe-samples, (top) HTP Fe-samples.

illustrated in Fig. 7 for Fe-FERs (Fe/Al 0.12; 0.26; 0.47), Fe-MFI_{0.11}, and Fe-BEA_{0.13}. In addition, the amounts of desorbed oxygen during the TPD runs after the batch interactions of nitrous oxide at $200\text{ }^\circ\text{C}$ also match this correlation. It thus follows that the area of the low-temperature TPR peak, as well as the amount of desorbed oxygen after interaction with N_2O interaction at $200\text{ }^\circ\text{C}$ (i.e., at the temperature at which formation of NO_x species, accelerating the molecular oxygen production, is negligible) can be directly correlated with the number of active sites for the N_2O decomposition. Accordingly, their number is substantially higher in Fe-FER than in Fe-BEA and Fe-MFI.

As concerns the recombination of O_{act} which is commonly assumed as the slowest reaction step, it can proceed either with the aid of framework oxygens (cf. the release of $^{16}O^{18}O$ during the decomposition of $N_2^{18}O$ —Fig. 6, and papers [23,29] or via the surface NO_x species [21–25], eventually by the reactions of another N_2O molecule with O_{act} . We regard it to be significant that, after high amounts of added NO, the three types of iron-zeolites exhibit quite similar N_2O conversion than without NO addition (Fig. 6). The active role of NO_x species (see Fig. 7) thus partially overwhelms the differences in the amount of active oxygens.

The similar composition of oxygen isotopomers with predominant $^{18}O^{16}O$ in the gas phase (Fig. 6) points to similar participation of zeolitic oxygens during the N_2O decomposition over all three Fe-zeolites. However, the number of active participating oxygens is relatively higher for Fe-BEA and Fe-MFI than for Fe-FER. Accordingly, the efficiency of the recombination of oxygens produced from decomposing nitrous oxide is higher in Fe-FERs.

Summarizing of the specific features of the N_2O -interaction with Fe-FER yields the following list of specific features:

- (i) high efficiency of active oxygen formation,
- (ii) unique catalytic activity in N_2O decomposition at temperatures below $400\text{ }^\circ\text{C}$,
- (iii) increase in the activity after the HTP treatment up to level attained by the addition of NO,
- (iv) minimum amount of NO necessary for the acceleration of the N_2O decomposition,
- (v) a high amount of accumulated NO_x species during the N_2O decomposition and its substantial increase after the HTP treatment.

As shown in the previous discussion, the difference between catalytic activities of the three zeolites could not be explained just by differences in the total amount of the cationic iron, and their specificity and differences from the other two zeolites must be analyzed.

Accordingly, the following discussion of this aspect is based on previous results of our group identifying nature of the cationic sites of divalent cations in the high silica zeolites (see also [35–39]), as well as our recent results of periodic DFT calculation of the Fe-FER structures with NO (see [18,19]) as well as with N_2O (Sklenák et al., to be published). The spatial arrangement of the iron cations in the high silica zeolites could just be summarized as follows:

- (i) The ion exchange of the divalent cations in high-silica zeolites results in occupation of three main cationic position, i.e. α , β , and γ positions, and these positions could be identified in the individual structures.
- (ii) There is a general tendency for the preferred occupation of the β position at low iron exchange levels, and this has been evidenced also for Fe-FER.

It follows that at low levels of iron exchange, as analyzed mostly in our study, high proportion of Fe(II) cations are situated in the β positions (to lower extent also in α positions), while by increasing the iron content other iron species must be also anticipated. The picture emerging from the Mössbauer spectroscopy, showing at low iron contents high proportion of Fe(II) related to preferential occupation of cationic positions, thus follows generally this pattern.

The analysis of the possible spatial arrangement of the iron cations, based on the above conclusions, indicated that in all three zeolites most of the iron cations would be situated in isolated extra framework positions. For these sites the possible Fe···Fe distance would be well above $8\text{ }\text{Å}$, and in some cases the iron cations in the nearest sites are facing to different channels. Accordingly, for such isolated sites there is only limited chance of two iron cations cooperation in any plausible way on the N_2O decomposition reaction. Moreover, the higher affinity for the iron cation for the nitrogen atom, as shown in analogy for interaction of NO with Fe-FER by Benco [18,19], would mostly provide the Fe···NNO complex and much less of the Fe···ONN, i.e. the complex potentially active for the formation of the Fe–O species.

On the other hand, using the same approach, we have identified one exception from such domination of isolated cationic sites, i.e. the local structure including two adjacent β sites facing each other across the channel (see Fig. 8). Actually, here the distance between two iron cations is about $7.5\text{ }\text{Å}$. Significantly, a strong attraction between the oxygen atom of Fe···NNO complex and the adjacent iron cation (distance $O\cdots Fe \sim 3\text{ }\text{Å}$) could be expected.

We propose that such local arrangement, which in the FER is quite realistic, could provide for N_2O splitting by mutual action of two adjacent iron cations Fe-FER, and can explain for the superior performance of Fe-FER both in capturing the O_{act} , as well as for N_2O decomposition itself.

A direct detection of the existence of the active site containing two close collaborating Fe(II) cations accommodated in the cationic sites of FER is beyond the present experimental capabilities of the structural techniques.

However, a simple evaluation of the probability of the existence of the active sites with such an arrangement of close Fe(II) cations using available experimental data [39] regarding the occupation of various cationic positions by divalent cations in the FER sample was employed. The results of this assessment strongly support our hypothesis regarding the active site containing two close collaborating Fe(II) cations located in the cationic sites. Our results show

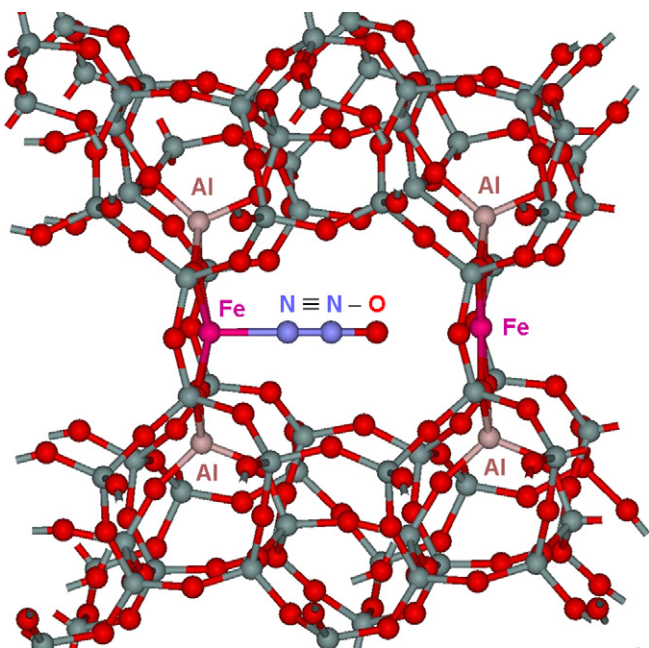


Fig. 8. Periodic DFT optimized structure of Fe-FER including N_2O interacting with two Fe cations occupying adjacent beta cationic positions.

that the close two Al atoms forming mainly β sites prevail in the FER framework [39]. If the iron exchange leads to a random occupation of the cationic sites then at least 5% contains two Al atoms in the β site balancing Fe(II) in the arrangement that a neighboring unit cell also accommodates Fe(II) in the β site, thus forming the active site containing two close collaborating Fe(II) cations accommodated in the cationic sites.

Such an arrangement of two Fe(II) cations located in the β sites of two neighboring unit cells allowing a formation of collaborating Fe(II) cations in Fe \cdots Fe pairs is quite unique and exists only for the FER sample used because of two reasons: the distribution of Al atoms in this FER framework as well as the optimal structural arrangement of the β sites in the FER framework.

In this connection, we would like to stress that these results do not eliminate the possibility that for highly loaded FER and for other zeolite structures the catalytic activity could be connected to other iron species, as proposed already in the literature (see, e.g., results of Panov's group).

5. Conclusions

The superiority of Fe-FER over Fe-BEA and Fe-MFI with Fe/Al ratios below 0.15 in the decomposition of nitrous oxide in the absence of NO has been established. It has been tentatively attributed to the presence of a unique FER structure containing two close collaborating Fe(II) cations accommodated in the cationic sites of FER. This local structure with unique spatial properties could, due to their distance and orientation, provide for N_2O splitting by mutual action of two adjacent iron cations in Fe-FER. This could explain the superior performance of Fe-FER both in capturing the O_{act} , as well as for N_2O decomposition itself.

Acknowledgments

Financial support of the grants No. 1ET400 400 413 of the AS CR and 1QS 400 400 560 of GA AS are highly appreciated.

References

- [1] G.I. Panov, V.I. Sobolev, A.S. Kharitonov, *J. Mol. Catal.* 61 (1990) 85.
- [2] V.N. Parmon, G.I. Panov, A. Uriarte, S. Noskov, *Catal. Today* 100 (2005) 115.
- [3] N. Hansen, A. Heyden, A.T. Bell, F.J. Keil, *J. Catal.* 248 (2007) 213.
- [4] Z. Sobalík, Transworld Research Network, Zeolites: From Model Materials to Industrial Catalysts 37/661 (2008) 333.
- [5] G.D. Pirngruber, P.K. Roy, R. Prins, *J. Catal.* 246 (2007) 147.
- [6] P.K. Roy, R. Prins, G.D. Pirngruber, *Appl. Catal. B Environ.* 80 (2008) 226.
- [7] I. Melián-Cabrera, C. Mentrui, J.A.Z. Pieterse, R.W. van den Brink, G. Mul, F. Kapteijn, J.A. Moulijn, *Catal. Commun.* 6 (2005) 301.
- [8] A.H. Oygarden, J.P. Pérez-Ramírez, *Appl. Catal. B Environ.* 65 (2006) 163.
- [9] J.A.Z. Pieterse, G.D. Pirngruber, J.A. van Bokhoven, S. Booneveld, *Appl. Catal. B Environ.* 71 (2006) 16.
- [10] J. Pérez-Ramírez, J.C. Groen, A. Brückner, M.S. Kumar, U. Bentrup, M.N. Debbagh, L.A. Villaescusa, *J. Catal.* 232 (2005) 318.
- [11] M. Mauvezin, G. Delahay, B. Coq, S. Kieger, J.C. Jumas, J. Olivier-Fourcade, *J. Phys. Chem. B* 105 (2001) 35.
- [12] K. Lázár, G. Lejeune, R.K. Ahedi, S.S. Shevade, A.N. Kotashane, *J. Phys. Chem. B* 102 (1998) 4865.
- [13] Z. Sobalík, J.E. Šponer, Z. Tvarůžková, A. Vondrová, S. Kuriyavar, B. Wichterlová, *Stud. Surf. Sci. Catal.* 135 (2001) 136.
- [14] B. Wichterlová, Z. Sobalík, J. Dědeček, *Appl. Catal. B Environ.* 41 (2003) 97.
- [15] J. Dědeček, D. Kaucký, B. Wichterlová, *Top. Catal.* 18 (2002) 283.
- [16] P. Sazama, J. Dědeček, V. Gábová, B. Wichterlová, G. Spoto, S. Bordiga, *J. Catal.* 254 (2008) 180.
- [17] M. Schwarze, Z. Sobalík, E.G. Caspary, D. Nižnanský, *Czechoslovak J. Phys.* 56 (Suppl. E) (2006) E147.
- [18] L. Benco, T. Bucko, R. Grybos, J. Hafner, Z. Sobalík, J. Dědeček, J. Hrušák, *J. Phys. Chem. C* 11 (2007) 586.
- [19] L. Benco, T. Bucko, R. Grybos, J. Hafner, Z. Sobalík, J. Dědeček, S. Sklenák, J. Hrušák, *J. Phys. Chem. C* 11 (2007) 9393.
- [20] S. Sklenák, Z. Sobalík, Z. Tvarůžková, B. Jansang, Ch. Li, F. Gao, B. Boekfa, L. Benco, T. Bucko, J. Hafner, *Proc. of the 4th Int. FEZA Conference*, 2008.
- [21] D. Kaucký, Z. Sobalík, M. Schwarze, A. Vondrová, B. Wichterlová, *J. Catal.* 238 (2006) 293.
- [22] J. Nováková, Z. Sobalík, *Catal. Lett.* 89 (2003) 243.
- [23] J. Nováková, Z. Sobalík, *Catal. Lett.* 105 (2005) 169.
- [24] J. Nováková, Z. Sobalík, *Catal. Lett.* 111 (2006) 195.
- [25] J. Nováková, Z. Sobalík, *Curr. Top. Catal.* 6 (2007) 55.
- [26] D.A. Bulushev, A. Renken, L. Kiwi-Minsker, *J. Phys. Chem. B* 110 (2006) 305.
- [27] CZ 293917 B6 (2001).
- [28] E. Galli, G. Vezzalini, S. Quartieri, A. Alberti, M. Franzini, *Zeolites* 19 (1997) 318; G. Vezzalini, S. Quartieri, E. Galli, A. Alberti, G. Cruciani, A. Kvicic, *Zeolites* 19 (1997) 323; J.M. Newsam, M.M.J. Treacy, W.T. Koetsier, C.B. de Gruyter, *Proc. R. Soc. London* A 420 (1988) 375.
- [29] J. Nováková, M. Schwarze, Z. Sobalík, *Catal. Lett.* 104 (2005) 157.
- [30] M.J. Nash, A.M. Shough, D.W. Fickel, D.J. Doren, R.F. Lobo, *J. Am. Chem. Soc.* 130 (2008) 2460.
- [31] S.N. Ovanesyanyan, A.A. Shteinman, A.K. Dubkov, I.V. Sobolev, I.G. Panov, *Kinet. Catal.* 39 (1998) 792.
- [32] S.N. Ovanesyanyan, A.K. Dubkov, A.A. Pyallin, A.A. Shteinman, *J. Radioanal. Nucl. Chem.* 246 (2000) 149.
- [33] A.K. Dubkov, S.N. Ovanesyanyan, A.A. Shteinman, V.E. Starokon, I.G. Panov, *Catalysis* 207 (2002) 341.
- [34] G.I. Panov, E.V. Starokon, L.V. Pirutko, E.A. Paukshtis, V.A. Parmon, *J. Catal.* 254 (2008) 110.
- [35] D. Kaucký, K. Jiřa, A. Vondrová, J. Nováková, Z. Sobalík, *J. Catal.* 242 (2006) 270.
- [36] J. Dědeček, L. Čapek, D. Kaucký, Z. Sobalík, B. Wichterlová, *J. Catal.* 211 (2002) 198.
- [37] D. Kaucký, A. Vondrová, J. Dědeček, B. Wichterlová, *J. Catal.* 194 (2000) 318.
- [38] J. Dědeček, D. Kaucký, B. Wichterlová, *Microporous Mesoporous Mater.* 35 (6) (2000) 483.
- [39] D. Kaucký, J. Dědeček, B. Wichterlová, *Microporous Mesoporous Mater.* 31 (1999) 75.